

DOI: 10.1002/cphc.200900053

## Reversible Structural Modulation of Fe–Pt Bimetallic Surfaces and Its Effect on Reactivity

Teng Ma, Qiang Fu,\* Hai-Yan Su, Hong-Yang Liu, Yi Cui, Zhen Wang, Ren-Tao Mu, Wei-Xue Li, and Xin-He Bao\*<sup>[a]</sup>

Bimetallic catalysts often present superior catalytic performance in comparison to their parent metals and have been widely used in many catalytic processes.<sup>[1–5]</sup> Compared with monometallic catalysts, bimetallic catalysts have more surface structural complexity, where the second metal—in either the metallic or the oxidized state—can be exposed on the surface, in the near surface region, or embedded in bulk region. It has been demonstrated that the surface structure of the bimetallic catalyst is critical to their catalytic properties. For example, Pt-based bimetallic catalysts consisting of Pt-skin surfaces with 3d transition metals at the subsurface region present super catalytic performances in many reactions compared to the pure Pt surface.<sup>[4,6–8]</sup> In order to optimize the catalytic performance, it is highly demanding to modulate the surface structure of the bimetallic catalysts. The structure of a catalyst surface often changes dynamically during reactions. For example, reversible surface processes such as wetting–dewetting and sintering–dispersion have been observed in monometallic catalyst systems when the gaseous environment changes between reductive and oxidative conditions.<sup>[9–11]</sup> The bimetallic catalysts may show similar dependence of surface structure on the redox potential of reaction gases, which offers eventually the opportunity to tune the catalytic activity and selectivity. Here, using well-defined Fe–Pt(111) systems we show that the surface structure of the bimetallic Fe–Pt catalysts can be indeed switched between the Pt-skin surface with Fe underneath and the iron oxide rich Pt surface. The reversible structural modulation regulated by cycled oxidation and reduction treatments exhibits feasible tunability in the surface CO adsorption strength and CO oxidation ability on the bimetallic catalysts.

Fe overlayers with coverage of about 1.0 monolayer (ML) were grown on a clean Pt(111) by molecular beam epitaxy with the substrate temperature at 487 K, producing a Fe/Pt(111) surface. Scanning tunnelling microscopy (STM), X-ray photoelectron spectroscopy (XPS), and ion scattering spectroscopy (ISS) [see Figure S1 in the Supporting Information (SI)] indicate that Fe grows on Pt(111) in the layer growth mode, at least for the first layer under the current deposition conditions. Upon an-

nealing a  $\sim 1.0$  ML Fe/Pt(111) surface in ultrahigh vacuum (UHV) at 850 K for 6 min, the surface Fe overlayers disappear completely, as indicated by the ISS spectrum (see Figure S2a in SI), where only Pt signals are present. This is confirmed further by the characteristic morphology of the atomically flat Pt(111) surface (Figure 1a and inset therein) by STM. However, XPS

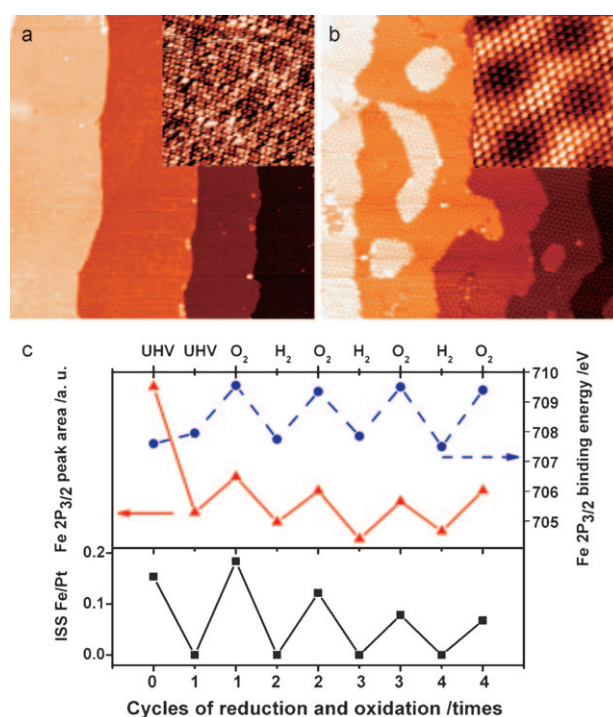


**Figure 1.** a) STM image ( $200 \times 200 \text{ nm}^2$ ) of Pt skin with subsurface Fe, Pt/Fe/Pt(111), obtained by annealing  $\sim 1.0$  ML Fe/Pt(111) at 850 K for 6 min, inset showing an atomic resolution image ( $10 \times 10 \text{ nm}^2$ ). b) STM image ( $200 \times 200 \text{ nm}^2$ ) of FeO/Pt(111) surface via annealing the Pt/Fe/Pt(111) surface from (a) in  $1.1 \times 10^{-6}$  mbar O<sub>2</sub> at 850 K for 6 min, inset showing an atomic resolution image ( $6.3 \times 6.3 \text{ nm}^2$ ). c) Variation of XPS Fe 2p<sub>3/2</sub> peak area, XPS Fe 2p<sub>3/2</sub> binding energy, and ratio of ISS Fe signal to Pt signal from a  $\sim 1.0$  ML Fe/Pt(111) surface upon cycled oxidation and reduction treatments.

measurements still show a strong signal from Fe (Figure S2b in SI), and a decrease of  $\sim 61\%$  in the Fe 2p<sub>3/2</sub> peak intensity occurs upon the UHV annealing. Considering that the attenuation of Fe 2p<sub>3/2</sub> photoelectrons through one layer Pt(111) is around 30%, Fe should diffuse into the near surface regions (mainly in first subsurface layer, around 0.5 ML) rather than the deep bulk. Correspondingly, the binding energy (BE) of Fe 2p<sub>3/2</sub> shifts from 707.2 eV for the surface Fe overlayers to 707.8 eV

[a] T. Ma, Prof. Q. Fu, H.-Y. Su, H.-Y. Liu, Y. Cui, Z. Wang, R.-T. Mu, Prof. W.-X. Li, Prof. X.-H. Bao  
State Key Laboratory of Catalysis  
Dalian Institute of Chemical Physics  
Dalian, Zhongshan Road 457, 116023 (P.R. China)  
Fax: (+86) 411-84686637  
E-mail: qfu@dicp.ac.cn  
xhbao@dicp.ac.cn

Supporting information for this article is available on the WWW under <http://dx.doi.org/10.1002/cphc.200900053>.

for the subsurface Fe due to the increase of the Pt–Fe coordination number. The produced Pt-skin surface with subsurface Fe underneath is noted as Pt/Fe/Pt(111).

The similar Pt-skin structures have been demonstrated in Cu/Pt(111),<sup>[7]</sup> Ni/Pt(111),<sup>[8,12]</sup> PtCo,<sup>[13]</sup> and Pt<sub>80</sub>Fe<sub>20</sub><sup>[14]</sup> bimetallic systems, where the 3d transition metals tend to diffuse into subsurface regions to form Pt-skin surfaces upon UHV annealing or in case of growth of the 3d metals at elevated temperatures. These Pt-skin structures have been shown to be promising catalysts for many reactions. However, the stability of the bimetallic catalysts under gaseous reaction environments remains unclear.<sup>[1,15]</sup> In order to study the change of the Fe–Pt(111) surface structure under different gas conditions, the Pt-skin surface was treated in the typical oxidative and reductive atmospheres, that is, O<sub>2</sub> and H<sub>2</sub>, respectively. The Pt/Fe/Pt(111) surface was first heated in 1.1 × 10<sup>-6</sup> mbar O<sub>2</sub> at 850 K for 6 min, and the surface morphology acquired via STM was shown in Figure 1 b. The surface now exhibits a superstructure with a periodicity of 25 Å, which is a typical Moiré pattern of two-dimensional monolayer FeO film grown on Pt(111).<sup>[16,17]</sup> The well-defined FeO atomic structure can be clearly discerned from the high resolution STM image (see inset in Figure 1 b). Moreover, a strong Fe signal is detected by ISS after the oxidation (Figure S2a in SI), which indicates the existence of Fe on the surface. At the same time, the intensity of XPS Fe 2p peak increases by ~45%, and the BE of Fe 2p<sub>3/2</sub> peak shifts up to 709.2 eV (Figure S2b in SI), which indicates the presence of the Fe(II) valence state of the segregated Fe. These results show unambiguously that the Pt/Fe/Pt(111) surface is not stable in O<sub>2</sub>, and subsurface Fe tends to segregate towards the surface and form an ordered FeO film on Pt(111) [noted as FeO/Pt(111)] upon oxidation. Subsequent annealing of the FeO/Pt(111) surface in 1.1 × 10<sup>-6</sup> mbar H<sub>2</sub> at 800 K for 6 min removes completely the surface O, and all surface Fe atoms diffuse into the subsurface region, which is accompanied by a shift of the Fe 2p<sub>3/2</sub> BE back to 707.8 eV. STM and ISS measurements indicate that the H<sub>2</sub>-annealed surface has the same surface structure and composition as Pt(111), namely, the Pt-skin surface, Pt/Fe/Pt(111), is resumed from FeO/Pt(111) upon the reduction.

More interestingly, the change between the surface Fe structure, FeO/Pt(111), and the Pt-skin structure, Pt/Fe/Pt(111), can be repeated via the cycled oxidation and reduction treatments. As shown in Figure 1 c, four cycles of oxidation and reduction have been conducted on a Fe–Pt(111) surface. Oxidation of each Pt-skin surface results in appearance of a strong Fe signal in the ISS spectra and an increase in the XPS Fe 2p<sub>3/2</sub> intensity along with a shift of Fe 2p<sub>3/2</sub> BE to around 709.2 eV, indicating the formation of FeO/Pt(111) surfaces. Starting with each FeO/Pt(111) surface, the Pt-skin surfaces can be regenerated via the reduction treatment, which was confirmed by absence of Fe signal in ISS spectra, decrease of XPS Fe 2p<sub>3/2</sub> intensity to ~60%, and shift of Fe 2p<sub>3/2</sub> BE to 707.8 eV. The Fe–Pt(111) surface shows a fully reversible change between the FeO covered Pt structure and the Pt-skin structure (Figure 1 c). The original Fe 2p<sub>3/2</sub> XPS spectra in the four cycles are presented in Figure S3 in SI. It should be noted that the similar reversible change in surface structure and composition of Fe–Pt bimetal-

lic catalysts was also observed in supported Fe–Pt nanoparticles (Figure S4 in SI).

Spin-polarized density function theory (DFT) calculations using ultrasoft pseudopotential plane wave and the GGA-PW91 method implemented in DACAPO package<sup>[18,19]</sup> are performed to study the stability of the Fe–Pt(111) surface under reductive and oxidative environments. The Fe–Pt(111) surface is modelled by substituting one Pt atom with Fe atom from the topmost Pt layer to the fourth Pt layer in the seven layer (2 × 2) Pt(111) slab separated by 15 Å vacuum (Figure 2 inset)

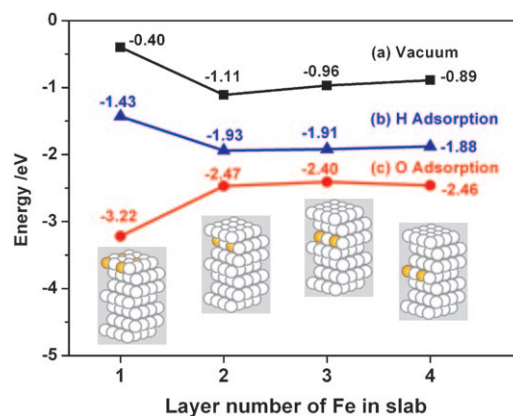


**Figure 2.** Relative stability of Fe–Pt bimetallic with Fe atom substituting one quarter Pt atom from the topmost Pt layer to the fourth Pt layer under the vacuum (a), H (b), and O adsorption (c) at coverage of 0.50 ML.

with full structural optimization. For the clean surface (Figure 2a), which corresponds to the condition in vacuum, the heat of formation,  $\Delta H$ , of Fe–Pt bimetallic surface with respect to the Pt(111) and bulk fcc Fe are plotted. When the Fe atom displaces from the topmost Pt layer to the subsurface Pt layer,  $\Delta H$  is lowered by 0.71 eV, but it increases gradually when the Fe atom moves into the deeper region. The result suggests that subsurface Fe below the topmost Pt layer is the most energetically favourable one. With hydrogen adsorption ( $\theta_{\text{H}} = 0.50$  ML) on the surface (Figure 2b), the relative stability of H-adsorbed Fe–Pt bimetallic surface by including the bonding energy between H and corresponding substrates does not change. These results agree well with surface-science experiments, where the Pt-skin surfaces with subsurface Fe are the most stable structure after annealing Fe–Pt samples under vacuum and H<sub>2</sub> conditions. Our calculations show that upon oxygen adsorption ( $\theta_{\text{O}} = 0.50$  ML), Fe–Pt bimetallic surface with Fe in the topmost Pt layer is the most stable, due to the significantly stronger O–Fe bonding than that of O–Pt, which eventually leads to Fe segregation and formation of the FeO monolayer on Pt(111), as found experimentally (Figure 1). The preference of subsurface Fe right below the topmost Pt layer under the reducing conditions and strong O–Fe interaction are the reason for the reversible change of the Fe–Pt surface structures during the oxidation and reduction cycles.

The oxidation and reduction treatments produce a Pt surface covered by iron oxide and Pt-skin surface with subsurface

Fe, respectively. Since the FeO structure formed on Pt(111) via the full oxidation treatments is inert to many gases, such as CO and O<sub>2</sub>, the reactivity of the FeO covered Pt(111) surface should behave as the pure Pt(111) surface. Therefore, we describe here a comparative reactivity study on Pt(111) and Pt-skin surfaces. First, CO and O adsorption on Pt(111) and Pt/Fe/Pt(111) were studied by high resolution electron energy loss spectroscopy (HREELS). Atomic O species were produced on both surfaces by adsorption of 100 L O<sub>2</sub> on Pt/Fe/Pt(111) and 30 L O<sub>2</sub> on Pt(111) at 110 K followed by annealing up to 300 K. On Pt(111) the HREELS spectrum shows one typical vibrational mode near 58.8 meV, which can be assigned to  $\nu(\text{Pt}-\text{O})$  mode of O on the 3-fold fcc hollow sites of Pt(111).<sup>[20]</sup> The vibrational mode of O on Pt/Fe/Pt(111) is similar to that on Pt(111), but the frequency presents a red shift by 3 meV relative to that on Pt(111), located at 55.8 meV (Figure 3a). Although weak ad-

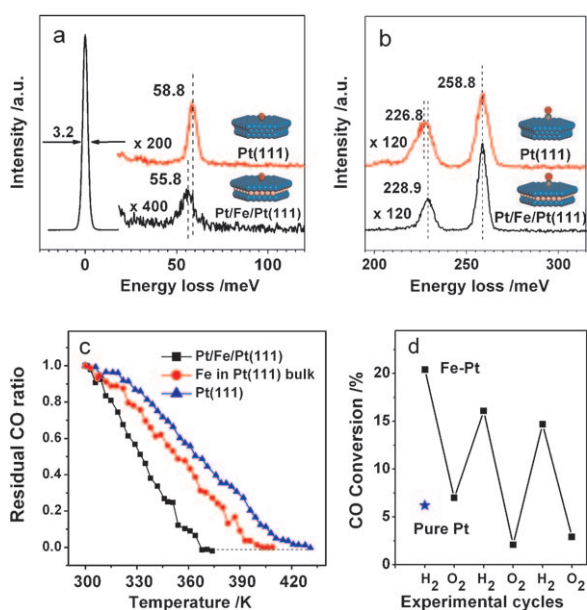


**Figure 3.** HREELS spectra of a) atomic O and b) CO adsorbed on Pt(111) and Pt/Fe/Pt(111), respectively. c) CO desorption from the Pt(111) surface, Pt/Fe/Pt(111) surface, and the Pt(111) with Fe in bulk. The CO desorption was monitored by TP-UPS. d) CO conversion for Pt/SiO<sub>2</sub> and Fe-Pt/SiO<sub>2</sub> catalysts in the PROX reactions at room temperature. Before each reaction, the Fe-Pt/SiO<sub>2</sub> catalysts were treated in flowing H<sub>2</sub> or O<sub>2</sub> gases at 623 K.

sorption of O on Pt skin surfaces has been reported previously from the ligand effect induced by subsurface Fe using DFT calculations,<sup>[21–23]</sup> our HREELS data present a first direct evidence for such an effect. The weaker adsorption on Pt/Fe/Pt(111) also explains why large O<sub>2</sub> exposure is applied to produce O on the surface. CO adsorption on the Pt(111) and Pt/Fe/Pt(111) surfaces at 110 K was also investigated by HREELS. Figure 3b displays the HREELS spectra of CO adsorption on both surfaces with 0.8 L CO exposure. The top-site adsorption on both surfaces has the similar frequency at 258.8 meV while the bridge-site adsorption of CO on Pt/Fe/Pt(111) shows a blue shift compared to the Pt(111), from 226.8 to 228.9 meV. The frequency shift for the bridge-site CO on Pt/Fe/Pt(111) is close to the cal-

culated value on a similar Pt skin structure of Pt<sub>80</sub>Fe<sub>20</sub> alloy,<sup>[24]</sup> which should be related to the weakened CO adsorption on Pt skin surface according to the classic Blyholder model.<sup>[25]</sup>

The variation of bond strength of CO on the Pt(111) and Pt-skin surfaces was further confirmed by temperature-programmed ultraviolet photoelectron spectroscopy (TP-UPS). Pt surfaces saturated by 6 L CO at 300 K were heated at the rate of 3 K/minute and monitored in-situ by He II UPS. The normalized intensity of the CO characteristic peak at 9.4 eV in the He II UPS spectra as a function of the sample temperature is plotted in Figure 3c and Figure S5 in SI. Complete desorption of CO on the Pt/Fe/Pt(111) surface occurs at around 370 K, while on Pt(111) CO desorbs slowly and disappears completely at about 430 K. In this context, we note that amount of subsurface Fe accumulated under reducing conditions is thermodynamically dependent. With increasing temperatures, the entropy effect becomes significant, and subsurface Fe atoms tend to diffuse further into the bulk region. The ligand effect induced by subsurface Fe on the reactivity of Pt-skin surface becomes weaker. Correspondingly, Pt-skin surface behaves like pure Pt. This is indeed verified by our experiments. By annealing as-prepared ~1 ML Fe/Pt(111) at 900 K for 6 min and exposing the same amount of CO, we found that CO desorbs completely at 405 K, which is higher than Pt/Fe/Pt(111) (370 K) due to the less amount of subsurface Fe, but remains lower than pure Pt(111) (430 K), as plotted in Figure 3c.

The surface adsorption and desorption results suggest that the presence of subsurface Fe at Pt(111) alleviates the poisoning by CO and makes dissociated O more reactive, which may enhance the catalytic activity with CO and/or O involved. To illustrate this, the performance of SiO<sub>2</sub> supported Pt and Fe-Pt nanoparticles were compared for the preferential oxidation reaction of CO (PROX) in excess of H<sub>2</sub>. The activity of the catalysts for CO PROX reaction (1% CO, 0.5% O<sub>2</sub>, 98.5% H<sub>2</sub>, 0.1 MPa, 36000 mLg<sup>-1</sup>h<sup>-1</sup>) was measured by performing the reactions at room temperature. For the Pt/SiO<sub>2</sub> catalyst only 6% CO conversion is observed, while the Fe-Pt/SiO<sub>2</sub> catalysts treated in H<sub>2</sub> (1 bar) at 623 K has much higher CO conversion, close to 20% (Figure 3d). Our experimental results show that the treatments of Fe-Pt(111) surface and supported Fe-Pt nanoparticles in H<sub>2</sub> could produce Pt-skin structure (Figure 1 and Figure S4 in SI). Thus, the higher CO conversion of Fe-Pt/SiO<sub>2</sub> catalysts pre-treated in H<sub>2</sub> should be attributed to the formation of Pt-skin surface, which decreases the CO poisoning and enhances the CO oxidation activity.<sup>[23]</sup> However, oxidation in O<sub>2</sub> drives the segregation of subsurface Fe to the top surface and results in a partial covering of Pt by iron oxides (Figure 1 and Figure S4 in SI). Thus, it is expected that the oxidized Fe-Pt catalysts should behave more like the pure Pt catalyst. Indeed, we observed that oxidizing the Fe-Pt/SiO<sub>2</sub> catalysts in O<sub>2</sub> (1 bar, 623 K) deteriorates the catalytic performance, showing CO conversion around 7%—close to that of pure Pt catalyst. Moreover, the alternating O<sub>2</sub> and H<sub>2</sub> treatments lead to up-down oscillations in CO conversion—high upon H<sub>2</sub> reduction but low after O<sub>2</sub> annealing. The reversible catalytic performance with the redox treatments is consistent with the structure change with O<sub>2</sub> and H<sub>2</sub> environments (Figure 1 and

Figure S4 in Support Information), showing the tunability of catalytic performance.

Dynamic change in the catalyst surface structures in response to variation in gaseous environments is one of the most important phenomena in heterogeneous catalysis and has been addressed in some catalyst systems.<sup>[1,9–11,26]</sup> In the present work, based on the comprehensive surface characterization data and theoretical contributions we have demonstrated that the Fe–Pt bimetallic catalyst presents the dynamic change in surface structure. The reversible structural modulation between the Pt skin surface and the iron oxide rich Pt surface can be induced by cycled oxidation and reduction. Furthermore, the reversible structural changes at Fe–Pt bimetallic catalyst surfaces results in tunability of the surface reactivities, such as PROX activity. The tunability of the surface structure and reactivity of bimetallic catalysts may open an effective way to design highly efficient catalysts for many important catalytic processes.

## Experimental Section

The surface experiments were performed in an Omicron Multiprobe surface science system, which is composed of sample preparation chamber, spectroscopic chamber, and microscope chamber. The Pt(111) is cleaned by cycles of 2.0 keV Ar<sup>+</sup> sputtering and annealing at 1000 K in UHV. The sample can be resistively heated up to 1100 K and cooled by liquid nitrogen down to 110 K. The Fe source is made of a coil of two 0.5 mm diameter tungsten wires wrapped with a 0.1 mm diameter Fe wire, and Fe coverage was determined by STM. All STM images are acquired at room temperature with a constant current mode of a tungsten tip. XPS measurement was performed with MgK $\alpha$  (1253.6 eV) using a pass energy of 30 eV. All ISS spectra were measured at He 5.0  $\times$  10<sup>-8</sup> mbar with 1.0 keV primary energy and the ion incidence angle of 50° with respect to the sample surface if not specially specified. The HREELS measurements are operated with the primary beam energy of 7.287 eV. The angles of incidence and reflection are 60 degree with respect to the surface normal in the specular direction. The gases of O<sub>2</sub>, CO, and H<sub>2</sub> (purity of 99.999%) are dosed into the system via sapphire leak valves.

The Pt and Fe–Pt nanoparticles supported on silica were prepared by a sol-gel method using H<sub>2</sub>PtCl<sub>6</sub> and Fe(NO<sub>3</sub>)<sub>3</sub> as the precursors. Through aging, nucleation, and subsequent H<sub>2</sub> treatment, Pt/SiO<sub>2</sub> and Fe–Pt/SiO<sub>2</sub> catalysts were produced, in which the loading of Fe and Pt was controlled at 4 wt.%. PROX reaction was conducted under the conditions of 1% CO, 0.5% O<sub>2</sub>, 98.5% H<sub>2</sub>, 0.1 MPa, and 36 000 mLg<sup>-1</sup>h<sup>-1</sup> at RT.

## Acknowledgements

This work was supported by the Natural Science Foundation of China (NSFC 20873143, 20603037, 20733008), Ministry of Science and Technology of China (MOST), and Chinese Academy of Sciences (CAS).

**Keywords:** bimetallic catalysts • carbon monoxide • dynamic processes • platinum • surface catalysis

- [1] J. G. Chen, C. A. Menning, M. B. Zellner, *Surf. Sci. Rep.* **2008**, *63*, 201.
- [2] M. Chen, D. Kumar, C.-W. Yi, D. W. Goodman, *Science* **2005**, *310*, 291.
- [3] J. Greeley, T. F. Jaramillo, J. Bonde, I. Chorkendorff, J. K. Norskov, *Nat. Mater.* **2006**, *5*, 909.
- [4] V. R. Stamenkovic, B. Fowler, B. S. Mun, G. Wang, P. N. Ross, C. A. Lucas, N. M. Markovic, *Science* **2007**, *315*, 493.
- [5] M. Heemeier, A. F. Carlsson, M. Naschitzki, M. Schmal, M. Baumer, H.-J. Freund, *Angew. Chem.* **2002**, *114*, 4242; *Angew. Chem. Int. Ed.* **2002**, *41*, 4073.
- [6] S. Alayoglu, A. U. Nilekar, M. Mavrikakis, B. Eichhorn, *Nat. Mater.* **2008**, *7*, 333.
- [7] J. Knudsen, A. U. Nilekar, R. T. Vang, J. Schnadt, E. L. Kunkes, J. A. Dumesic, M. Mavrikakis, F. Besenbacher, *J. Am. Chem. Soc.* **2007**, *129*, 6485.
- [8] L. E. Murillo, A. M. Goda, J. G. Chen, *J. Am. Chem. Soc.* **2007**, *129*, 7101.
- [9] Y. Nishihata, J. Mizuki, T. Akao, H. Tanaka, M. Uenishi, M. Kimura, T. Okamoto, N. Hamada, *Nature* **2002**, *418*, 164.
- [10] P. L. Hansen, J. B. Wagner, S. Helveg, J. R. Rostrup-Nielsen, B. S. Clausen, H. Topsøe, *Science* **2002**, *295*, 2053.
- [11] P. Nolte, A. Stierle, N. Y. Jin-Phillipp, N. Kasper, T. U. Schulli, H. Dosch, *Science* **2008**, *321*, 1654.
- [12] J. R. Kitchin, N. A. Khan, M. A. Barteau, J. G. Chen, B. Yakshinskiy, T. E. Madey, *Surf. Sci.* **2003**, *544*, 295.
- [13] V. R. Stamenkovic, B. S. Mun, K. J. J. Mayrhofer, P. N. Ross, N. M. Markovic, *J. Am. Chem. Soc.* **2006**, *128*, 8813.
- [14] C. Creemers, P. Deurinck, *Surf. Interface Anal.* **1997**, *25*, 177.
- [15] C. A. Menning, H. H. Hwu, J. G. Chen, *J. Phys. Chem. B* **2006**, *110*, 15471.
- [16] W. Weiss, M. Ritter, *Phys. Rev. B* **1999**, *59*, 5201.
- [17] L. Giordano, G. Pacchioni, J. Goniakowski, N. Nilius, E. D. L. Rienks, H.-J. Freund, *Phys. Rev. B* **2007**, *76*, 075416.
- [18] B. Hammer, L. B. Hansen, J. K. Norskov, *Phys. Rev. B* **1999**, *59*, 7413.
- [19] J. P. Perdew, J. A. Chevary, S. H. Vosko, K. A. Jackson, M. R. Pederson, D. J. Singh, C. Fiolhais, *Phys. Rev. B* **1992**, *46*, 6671.
- [20] H. Steininger, S. Lehwald, H. Ibach, *Surf. Sci.* **1982**, *123*, 1.
- [21] Y. Xu, A. V. Ruban, M. Mavrikakis, *J. Am. Chem. Soc.* **2004**, *126*, 4717.
- [22] M. P. Hyman, J. W. Medlin, *J. Phys. Chem. C* **2007**, *111*, 17052.
- [23] H.-Y. Su, X.-H. Bao, W.-X. Li, *J. Chem. Phys.* **2008**, *128*, 194707.
- [24] R. Hirschl, F. Delbecq, P. Sautet, J. Hafner, *Phys. Rev. B* **2002**, *66*, 155438.
- [25] G. Blyholder, *J. Phys. Chem.* **1964**, *68*, 2772.
- [26] F. Tao, M. E. Grass, Y. Zhang, D. R. Butcher, J. R. Renzas, Z. Liu, J. Y. Chung, B. S. Mun, M. Salmeron, G. A. Somorjai, *Science* **2008**, *322*, 932.

Received: January 23, 2009

Published online on April 27, 2009